The Delayed Response of Airborne Thermometers: Part 1: Determining the Characteristic Response

William A. Cooper and others...

DRAFT March 2020

National Center for Atmospheric Research
Earth Observing Laboratory
Research Aviation Facility

Table of Contents

List of Figures

List of Tables

Preface and Abstract

The time response of some standard airborne thermometers is determined by observing the transfer function where the known input is turbulent dynamic heating. Differential equations for the response are proposed, and it is verified that the solutions to those differential equations provide good representations of the response characteristics in terms of fitted empirical coefficients. Those solutions then can be used to correct the measurements to compensate in part for the response characteristics of the sensors.

Acknowledgments

This material is based upon work supported by the National Center for Atmospheric Research, which is a major facility sponsored by the National Science Foundation under Cooperative Agreement No. 1852977. Any opinions, findings and conclusions or recommendations expressed in this publication are those of the author(s) and do not necessarily reflect the views of the National Science Foundation. The data used in the examples presented are from the VOCALS (VAMOS Ocean-Cloud-Atmosphere-Land Study), SOCRATES (Southern Ocean Clouds, Radiation, Aerosol Transport Experimental Study) and the CSET (Cloud Systems Evolution in the Trades) experiment, each described at this URL. Citations for the data sets are included in the references. Measurements (UCAR/NCAR - Earth Observing Laboratory [2011], UCAR/NCAR - Earth Observing Laboratory [2019], UCAR/NCAR - Earth Observing Laboratory [2018]) were collected by the project experiment teams, and flight operations and data acquisition and processing were performed by the Research Aviation Facility, Earth Observing Laboratory, National Center for Atmospheric Research (NCAR). The analyses reported here were mostly performed using R (R Core Team [2019]), with RStudio (RStudio [2009]) and knitr (Xie [2013, 2014]). Data files in netCDF format have been read and written using the R package "ncdf4"; cf. Pierce [2015]. Substantial use also was made of the "ggplot2" package (Wickham [2009]) for R, and some fits relied on the "nleqslv" package for R Hasselman [2018]. Extensive use was made of the "stats" package, part of Core R. Some of the numerical integrations used the Runge-Kutta function from the "rmutil" package (Swihart and Lindsey [2019]).

1 Introduction

1.1 Overview

Various recent reviews of priorities for research in atmospheric science have called attention to the important roles that fluxes of various quantities play in climate science and have advocated increased focus on those fluxes; e.g., National Research Council [1998]. Among the fluxes that should be measurable using research aircraft is the flux of sensible heat. That requires, for the standard eddy-correlation measurement, that temperature be measured with sufficient response to resolve the spectrum of contributions to the flux. Temperature is a routine measurement on research aircraft, but most sensors do not have adequate response for this measurement. This set of three papers argues that application of a correction procedure developed in the third paper improves this measurement sufficiently to make it reliable despite the response-characteristics of airborne thermometers. That paper relies on information from the first two.

In this first paper, the time response of some standard airborne temperature sensors is characterized in terms of a transfer function that relates the measurand (the temperature) to the measurement (the sensor output) in ways that are invertible. Two coupled differential equations are used as the basis for this characterization, but the transfer function is determined independent of those equations. Because the equations predict a transfer function matching the observations, they provide a useful generalization of that transfer function.

Some aspects of the uncertainty limits associated with temperature as measured from research aircraft are included in an NCAR Technical Note (Cooper et al. [2016]), which was focused on the measurements of wind from the NSF/NCAR Gulfstream V research aircraft, hereafter called the GV. That aircraft and a C-130 are owned by the National Science Foundation (NSF) and operated by the Research Aviation Facility (RAF), Earth Observing Laboratory (EOL), National Center for Atmospheric Research (NCAR). The NCAR Technical Note included an estimate that the standard uncertainty in measurements of temperature from the GV is about 0.3°C and referenced Cooper et al. [2014] for supporting evidence. This limit applies when the temperature being measured is varying slowly and does not consider apply when the temperature changes rapidly. It is well known, however, that temperature sensors in common use on research aircraft have time-response characteristics that can affect the measurements. Friehe and Khelif [1992] and Lawson and Rodi [1992], among many others, provide reviews of the evidence for delayed response of the standard sensors. In particular, the unheated Rosemount 102E4AL sensor has been used widely as a fast-responding sensor, but its response characteristics are inadequate for many applications on a fast-moving aircraft like the NSF/NCAR GV.

The time response of temperature sensors becomes particularly important when it is desired to measure the flux of sensible heat (F_s) by the eddy-correlation method. The basis for this measurement is this equation:

$$F_s = \rho_a \, C_p \, \langle w'T' \rangle \tag{1}$$

where ρ_a is the density of air, C_p the specific heat of air at constant pressure, w the vertical wind, and T the temperature. Primes in this equation denote fluctuations from the mean and angle brackets denote an ensemble average. The measurement thus depends on having a temperature sensor that can respond to the range of fluctuations making significant contributions to the heat flux. Friehe and Khelif [1992] suggest, without demonstration, that 4–5 Hz is "just adequate" (for flight at around 125 m/s) and that 25 Hz would be desirable to resolve some interesting aspects of the temperature structure. If the response of the temperature sensor is reduced or shifted in phase at a particular frequency, an error will be introduced into the measurement of sensible-heat flux. Lawson and Rodi [1992] argued that sensible-heat flux measured by some of the fastest sensors in common use produced measurements of sensible heat flux about 21% too low compared to the measurements from their faster thermocouple-based sensor. It therefore is essential, for this measurement, to characterize the time response of the temperature sensor used and, where necessary, to apply corrections to compensate for that response.

This paper develops a new method for evaluating of the time response of a temperature sensor and applies that method to some temperature sensors now used on research aircraft. One significant difference in comparison to previous studies by, e.g., McCarthy [1973] and Inverarity [2000], is that the correction is applied to the measurement from the sensor, which corresponds to the "recovery temperature", rather than the final temperature after correction for dynamic heating. The latter reference addresses this but removes the dynamic-heating correction prior to applying a correction scheme. Because the sensor cannot respond to rapid fluctuations in dynamic heating, the standard correction for dynamic heating introduces errors into the sensed temperature that are then amplified by a correction procedure. This will be addressed in Part II.

Payne et al. [1994] provided a particularly illuminating analysis of the expected response of a temperature sensor and developed their results in terms of a transfer function. They represent the response of the sensor in terms of two coupled differential equations, one representing the temperature of the sensing wire and a second representing the temperature of the structure that supports that wire. Their analysis in terms of fundamental representation of the heat transport leads to reasonable consistency with previous two-time-constant models like that of McCarthy [1973] but poor agreement with the empirical evidence regarding the time-response parameters in those models. They note, however, that the empirical evidence is not as consistent or convincing as would be desirable. One goal of the present work, therefore, is to develop a different and readily available method of determining those parameters. The over-arching goal is to be able to assess errors that might be present in measurements of the flux of sensible heat and to apply corrections for those errors. The transfer function, constrained by new data regarding the parameters, makes this possible and also supports a new scheme by which the temperature measurements can be corrected for the time response of the sensor. This will be the subject of Part III.

1.2 Basis for the Assessment

The evaluation of the time response that follows uses several methods, but the key one is based on the dynamic heating produced by airspeed fluctuations. In steady conditions a temperature sensor exposed to the air stream will measure the recovery temperature, defined as the ambient temperature increased by the effect of dynamic heating. Dynamic heating fluctuates as the airspeed fluctuates, so in a turbulent wind field fluctuations with a measurable frequency spectrum are imposed on the sensor. These fluctuations are often significantly larger than real fluctuations in the ambient temperature. If the fluctuations are higher in frequency than those to which the sensor can respond, corresponding fluctuations will not appear in the measured spectrum. Furthermore, the phase of the measured response relative to the imposed signal will vary, from near 0° for fluctuations slow compared to sensor response to near 90° or even more[1] for fluctuations fast compared to that response. The amplitude and especially the phase of the recovery temperature relative to that of the dynamic heating therefore can be used as sensitive indicators of the response characteristics of the sensor.

The evaluation in terms of the amplitude ratio and phase shift of the recovery temperature as forced by the dynamic-heating term will therefore be the central approach in this study. Two other sources of information also provide supporting evidence. Those are: (i) the observed time delay during "speed-run" maneuvers, during which the flight speed is changed between minimum and maximum values; and (ii) passage through a near-discontinuous change in temperature at the top of a marine boundary layer. On the basis of this evidence, it will be argued that current standard temperature sensors do not meet the requirement even of 4–5 Hz response. Measurements of sensible heat flux will underestimate the contributions from fluctuations even as slow as 0.05 Hz, and the measured fluctuations lead to measurements of the contribution from 10-Hz fluctuations that are smaller than 10% of the correct values. Knowledge of the limitations of these sensors is therefore essential to any application to measurements of sensible heat flux that uses these sensors, and the correction schemes developed in Part III can lead to defensible measurements of sensible-heat flux that otherwise will have serious errors.

[1] A sensor with a first-order time constant cannot produce a phase lag of more than 90°, but larger lags are possible for systems characterized by two time constants, as developed below.

2 Characterizing the Time Response

2.1 The differential equations and their solution

Previous studies have demonstrated that a simple first-order response with one time constant does not represent the nature of existing sensors. The suggested explanation (Lenschow [1972] is that heat is transferred to the sensing wire of standard sensors not only from the air but also from the support that is in contact with the wire. Friehe and Khelif (Friehe and Khelif [1992]), following other prior work including that of McCarthy [1973], suggested representing the two-time-constant response via the following functional form:

$$\Theta(t) = A_1 e^{-t/\tau_1} + A_2 e^{-t/\tau_2} \tag{2}$$

where $\Theta(t)$ is the normalized history of the measured temperature decaying from an initial value of unity to a final value of zero. The sum of the coefficients A_1 and A_2 must then be 1. Suggested values for $\{A_1,\ A_2,\ \tau_1,\ \tau_2\}$ were $\{0.65,\ 0.35,\ 0.09\ \text{s},\ 0.5\ \text{s}\}$.

To consider how a sensor responds to a general input and not just to the step-function change described by (2), an appropriate pair of differential equations is developed and solved in this section. Following the approach of Payne et al. [1994], the following represents the time response of the sensor in terms of two coupled differential equations, one that describes the response of the support to the air temperature and a second that describes the response of the sensing wire to two inputs, one from the support and one from the air. No attempt is made to determine the parameters from first principles as in that reference, however; instead, parameters entering the equations are determined empirically. This approach leads to the following two differential equations describing the temperature of the support[2] ($T_s(t)$) and of the sensing wire ($T_m(t)$) as they respond to the measurand that is the recovery temperature ($T_r(t)$):

$$\frac{dT_s(t)}{dt} = \frac{T_r(t) - T_s(t)}{\tau_2} \tag{3}$$

$$\frac{dT_m(t)}{dt} = \frac{a(T_r(t) - T_m(t)) + (1-a)(T_s(t) - T_m(t))}{\tau_1} = \frac{\{aT_r(t) + (1-a)T_s(t)\} - T_m(t)}{\tau_1} \tag{4}$$

For heat transfer to or from the wire, the parameter a then represents the fraction of the heat conducted by the air, while a fraction $(1-a)$ is transferred to or from the support. The wire responds to the combined transfers of heat with characteristic time constant τ_1 while the support structure responds to the air temperature more slowly, with time constant τ_2. It is straightforward to apply (3) and (4) to changing but not necessarily discrete conditions, so a general response to a given air-temperature history

[2] A heat-transfer term omitted from the first equation is that from the support to the wire, which is assumed a negligible effect on the support temperature.

can be predicted by numerical integration of these equations.[3] The first does not involve the measurement, so for a particular history of recovery temperature $T_r(t)$ the support temperature can be determined solely by integration of (3). Then, with $T_s(t)$ determined, (4) can be integrated to find the expected measurement $T_m(t)$ for a specified history $T_r(t)$. The inverse process, finding $T_r(t)$ from the measurements $T_m(t)$, is also straightforward and only slightly more complicated, as discussed in Sect. 4.

For a sine-wave input, these equations have analytic solutions after any transient response from initial conditions has decayed. If the actual recovery temperature is $T_r(t) = \sin \omega t$ where ω is the angular frequency, then the solutions for $T_s(t)$ and $T_m(t)$ are given by the following equations:

$$T_s(t) = b \sin(\omega t + \zeta) \tag{5}$$

$$T_m(t) = c \sin(\omega t + \phi) = C_1 \cos \omega t + C_2 \sin \omega t \tag{6}$$

where

$$b = \frac{1}{\sqrt{1 + \omega^2 \tau_2^2}}$$

$$\zeta = -\arctan(\omega \tau_2)$$

$$C_1 = \left(\frac{1}{1 + \omega^2 \tau_1^2} \right) \left(-\omega \tau_1 \left(a + (1-a) b \cos \zeta \right) + (1-a) b \sin \zeta \right)$$

$$C_2 = \left(\frac{1}{1 + \omega^2 \tau_1^2} \right) \left(a + (1-a) b \cos \zeta + \omega \tau_1 (1-a) b \sin \zeta \right)$$

$$c = \sqrt{C_1^2 + C_2^2} \tag{7}$$

$$\phi = \arctan(C_1 / C_2) \tag{8}$$

The transfer function $H(\omega) = c(\omega) e^{i\phi(\omega)}$ then describes how the sensor will respond to a unit-amplitude sine wave with angular frequency $\omega = 2\pi\nu$ where ν is the frequency.[4]

2.2 The transfer function

Equations (7) and (8) provide the gain and phase for the time-response transfer function of the sensor. For a particular set of parameters (a =0.733, τ_1 =0.0308 s, τ_2 =0.447 s), the amplitude response and phase delay of the transfer function obtained in this way is shown in Fig. 1. These parameters are approximately representative of an unheated Rosemount

[3] The step-function response of (3) and (4) is the sum of two exponentials as in (2), with the same time constants but with the adjustment that $A_1 = (a - \tau_1/\tau_2)/(1 - \tau_1/\tau_2)$ and $A_2 = (1-a)/(1 - \tau_1/\tau_2)$. Because τ_1 is normally small compared to τ_2 for the Rosemount 102E4AL sensor, $A_1 \approx a$..

[4] The workflow document that accompanies this technical report develops and checks these solutions using Laplace transforms, but they have also been verified by substitution into the differential equations.

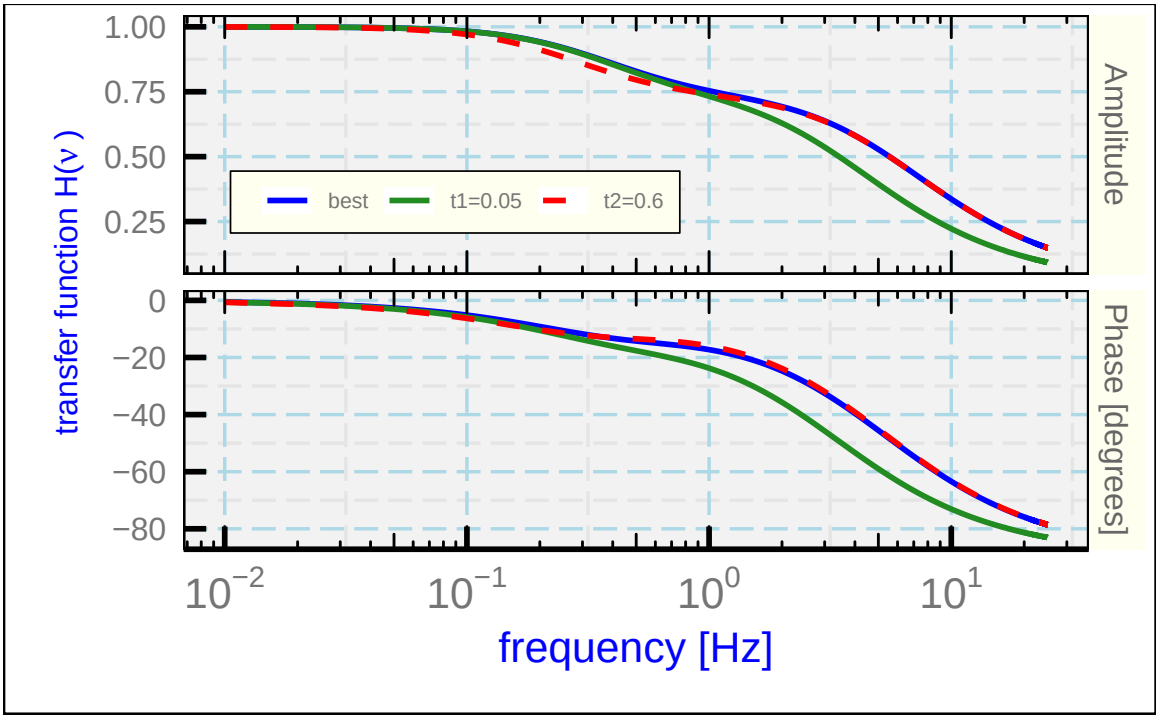

Figure 1: The amplitude and phase for the response function of the Rosemount 102E4AL temperature sensor. The parameters representing that sensor, labeled "best", are a=0.733, $\tau_1 = 0.0308$ s and $\tau_2 = 0.447$ s. To illustrate sensitivity, the curves labeled "t1=0.05" and "t2=0.6" use instead $\tau_1 = 0.05$ s and $\tau_2 = 0.6$ s, respectively.

102E4AL sensor that has been used on the NSF/NCAR C-130, as will be demonstrated in Sect. (3.1.1). The sensor in effect acts as a filter with the plotted gain and phase, so the frequency-dependent gain and phase can be used with Fourier representation of an input signal to characterize the response of the sensor to that input. Modified transfer functions for two small changes to these parameters are also shown to illustrate the sensitivity of the solution to these parameters. This figure illustrates that serious errors will enter estimates of the sensible heat flux if there are significant contributions at frequencies even above about 1 Hz. Because the contribution to the cospectrum of temperature and vertical wind will be reduced by the product of the amplitude and the cosine of the phase shown in Fig. 1, the fractional error in the measurement will be as shown in Fig. 2. Most of the 10-Hz contribution is missed, but even at 1 Hz the error is about 28%. If there are substantial contributions to the sensible-heat flux with fluctuations at 1 Hz and above, the fractional error in those contributions will lead to an error in the measured flux.

These equations and their solution also provide a basis for correcting either the measured temperature or the sensible-heat flux calculated from the cospectrum in (1). Corrected values can be obtained by integration of the equations for the derivatives, as by McCarthy [1973] or Inverarity [2000], or by using Fourier transforms and the transfer function. Before discussing those correction schemes in more detail, an analysis is needed to find the three parameters $\{a, \tau_1, \tau_2\}$. That is the subject of the next section. Then correction schemes are discussed further in Sect. 4.

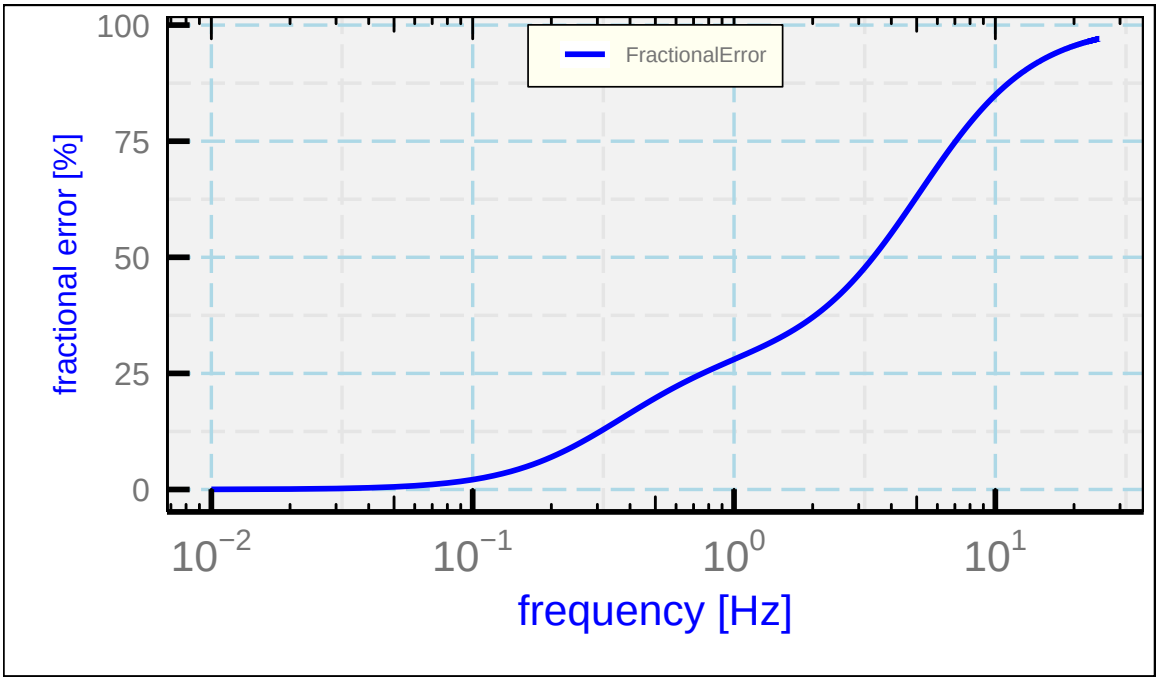

Figure 2: Fractional error in the contribution to sensible heat flux as a function of frequency.

3 Determining the Time Constants

3.1 The response to dynamic heating

3.1.1 The unheated Rosemount 102E4AL sensor

Dynamic heating provides an opportunity to evaluate the sensor response because that dynamic heating is a measured signal and its magnitude often is large compared to real temperature fluctuations. Dynamic heating of temperature sensors is discussed for example by Bange et al. [2013] (cf. their Eq. 2.23) and also in the working document describing processing algorithms in use at the Research Aviation Facility, NCAR: "RAF Technical Report: Processing Algorithms". These sources express dynamic heating Q as

$$Q = \alpha_r \frac{V^2}{2C_p} = T_r \left(\frac{\alpha_r M^2 R_a/(2C_v)}{1 + \alpha_r M^2 R_a/(2C_v)} \right) \tag{9}$$

where α_r is the "recovery factor" characterizing the extent to which the air is brought to rest relative to the sensor, V is the airspeed, C_p and C_v are respectively the specific heat of air at constant pressure and constant volume, T_r is the (true) recovery temperature expressed in absolute units, M the Mach number, and R_a the gas constant for air. The ambient air temperature T_a is related to the recovery temperature and the dynamic heating via

$$T_r = T_a + Q \ . \tag{10}$$

Dynamic heating can exceed 20°C at jet-aircraft flight speeds, so the large correction is often the dominant cause of fluctuations in the recovery temperature. The observed phase and amplitude of the measured response to that forcing should conform to the predictions of the transfer function. When fluctuations in the dynamic-heating term are the dominant cause of fluctuations in the recovery temperature, theoretical predictions like that shown in Fig. 1 can be used to determine appropriate values of characteristic parameters like a , τ_1 and τ_2 that fit the predictions to the observations.

Because the airspeed V is itself conventionally determined using the processed air temperature T_a, via $V = M\sqrt{\gamma R_a T_a}$ where $\gamma = C_p/C_v$, the second expression in (9) provides the advantage that it does not rely on prior calculation of the air temperature T_a but can be calculated from only the recovery temperature T_r and the Mach number. The Mach number in turn depends only on measurements of the dynamic and ambient pressures, with a small adjustment for the water vapor pressure. The goal here is to use the phase of the response to the dynamic-heating term to determine the response characteristics of the temperature sensor, so it is preferable to remain as close to the original measurements as possible.

The available measurement is not the true recovery temperature T_r, however, but instead the measured temperature T_m which may not include high-frequency fluctuations in T_r. This in turn affects the estimated fluctuations determined from (9). To minimize this problem, regions were sought where the fluctuations in dynamic heating were the dominant cause of fluctuations in recovery temperature. Temporarily consider these approximations: $\alpha_r \approx 1$, $R_a/(2C_v) \approx 1/5$, and M small enough that the denominator of the right side of (9) can be assumed equal to unity. Dynamic heating then is approximately $Q \approx T_r M^2/5$ and fluctuations in Q are related to those in T_r and M according to

$$\frac{\delta Q}{Q} \approx \frac{\delta T_r}{T_r} + \frac{2}{5}\frac{\delta M}{M} \tag{11}$$

The measured recovery temperature T_m may not include true high-frequency fluctuations in T_r, so the measured phase and amplitude of the response to the dynamic-heating term may be distorted from the correct value at frequencies where $\delta T_m/T_m$ differs from $\delta T_r/T_r$. In regions where the last term in (11) dominates, underestimation of the fluctuations in the recovery temperature arising from sensor response will cause less significant errors in the measured fluctuations in dynamic heating Q, but these errors still must be addressed.For this reason, once a set of parameters is determined, $T_r(t)$ can be estimated from the correction procedure outlined in Sect. 2.2.[5] Iteration using this estimate of $T_r(t)$ in place of $T_m(t)$ can then improve the estimate of the parameters. In practice, the estimate became stable after only one or two iterations.

To illustrate this process, consider a low-level flight segment from the VOCALS project where modest turbulent fluctuations were encountered. The primary temperature sensor for this project was an unheated Rosemount 102E4AL sensor. Figure 3 shows the variance spectrum for measurements of airspeed in this region. While the shape is not ideal for an inertial sub-range, it is close with an indicated eddy dissipation rate of about 3 ×

[5]See also section 4.

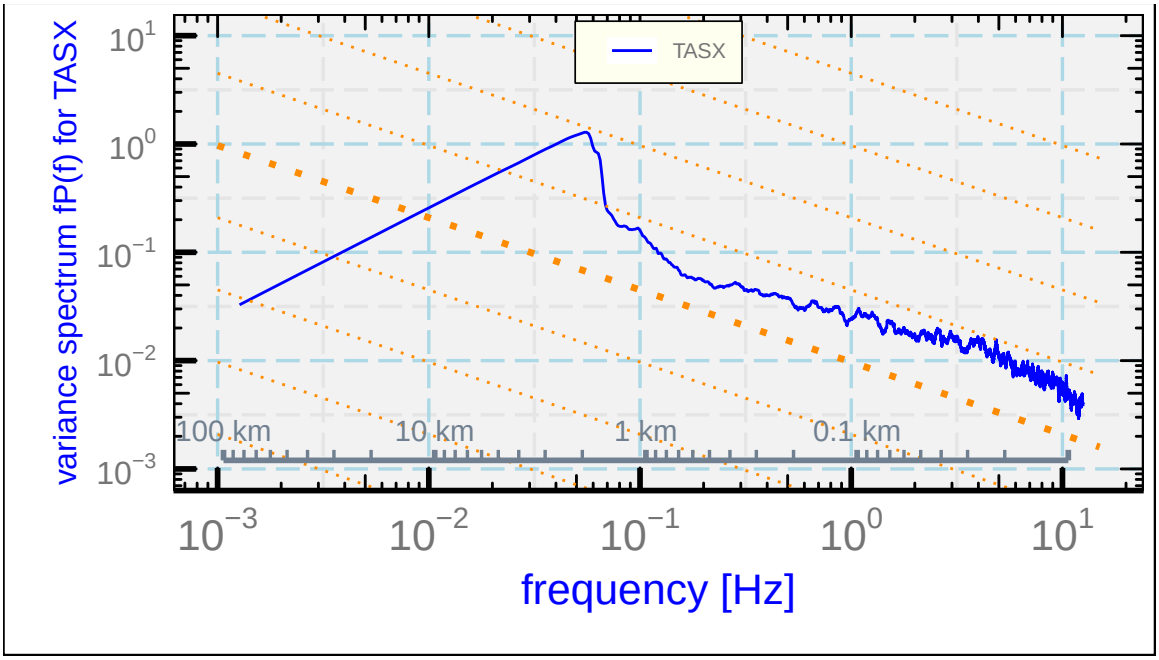

Figure 3: Variance spectra for airspeed from a segment from VOCALS C-130 flight 3, 11:39:00 – 11:52:00 UTC. The dotted orange lines show the spectral variance for various values of the eddy dissipation rate, with the heavy-dotted line representing 10^{-4} m^2 s^{-3}.

$10^{-4}\,\mathrm{m^2 s^{-3}}$. Figure 4 shows the contributions to the dynamic-heating term from the two terms on the right side of (11), except that T_m is used instead of the unknown T_r. The variance of the second term is more than 100 times that of the first, indicating that the fluctuations in the first term are less than 10% of those in the second term. Therefore the right side of (9) with T_m in place of T_r was used initially to represent dynamic heating and determine the transfer function representing the response to the imposed dynamic heating.

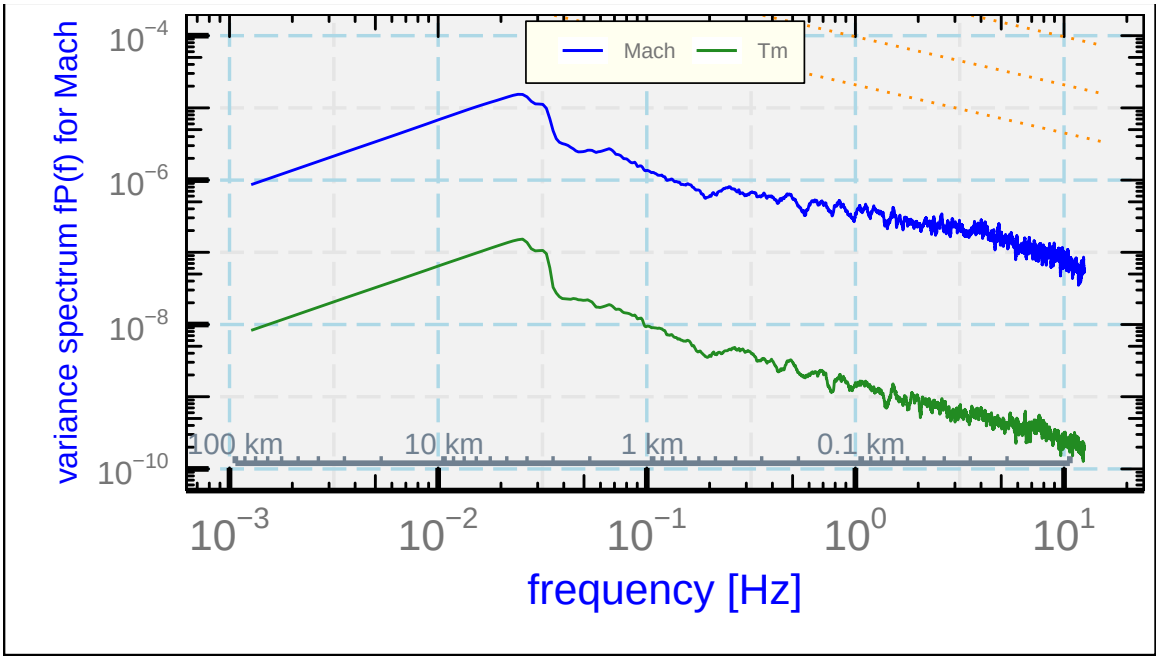

Figure 4: Spectral variance for $\delta T_m/T_m$ and $0.4\delta M/M$ for the same flight segment shown in the previous figure. The two terms are labeled "Tm" and "Mach" in the legend.

Segment	start	end
1	6:50:00	7:00:00
2	7:33:00	7:43:00
3	10:46:00	10:56:00
4	11:42:00	11:52:00
5	12:43:00	12:53:00
6	13:30:00	13:40:00

Table 1: Flight segments from flight 3 of the VOCALS project, 21 October 2008. Listed times are UTC.

To extend this analysis to a larger data set, six ten-minute low level flight segments in the marine boundary layer from one flight of the NCAR/NSF C-130 were selected that had simular flight conditions including the intensity of the turbulence. The time intervals are listed in Table 1. For each flight segment, the phase and amplitude ratio between the measurement and the dynamic heating term were calculated,[6] and the results for all six segments were averaged in 200 logarithmically spaced intervals in frequency. The results for the average phase are shown in Fig. 5. The error bars in that figure indicate the two-standard-deviation limits of those mean values. The theoretical curve is based on best-fit parameters as determined from these measurements and those of the amplitude ratio, discussed next.

The ratio of the amplitude of the response to that of the dynamic-heating signal, used as an

[6]The R routine "spec.pgram()" was used with 25-point modified Daniell smoothing.

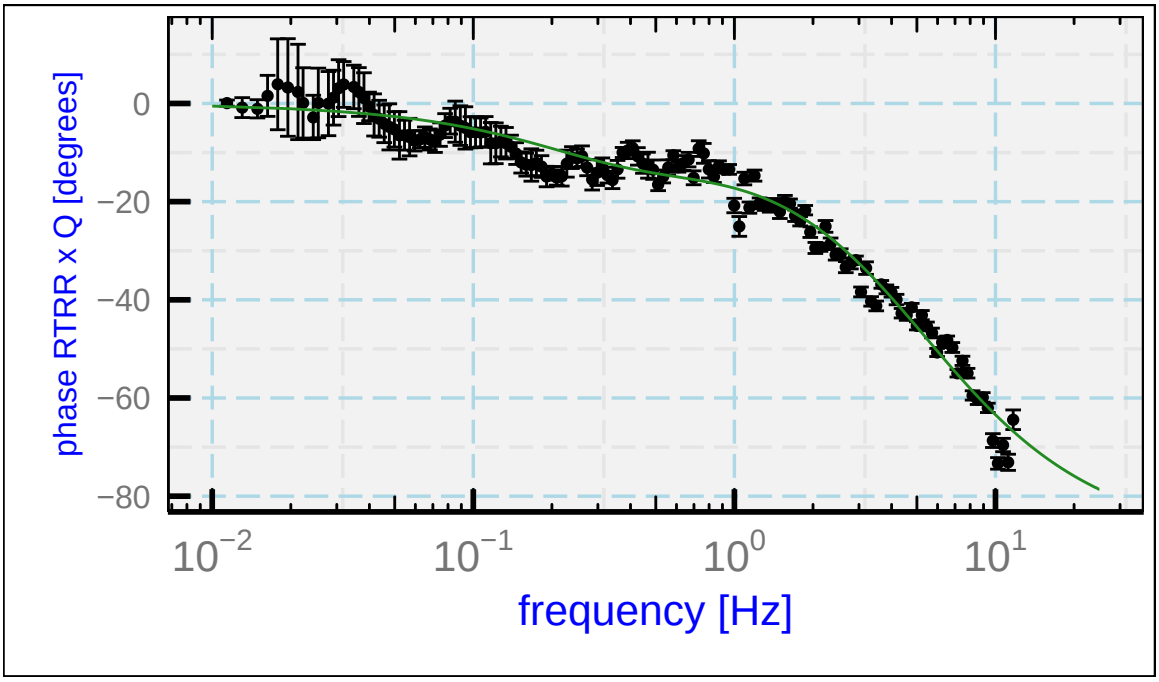

Figure 5: Phase lag of recovery temperature behind dynamic heating, for the measurements (error bars) and for the theoretical response for the best-fit parameters (green line). Data from the VOCALS project, flight 3, flight segments as in Table 1.

estimate of the gain of the transfer function, is shown in Fig. 6. It is useful to consider both the amplitude and phase when determining the response parameters because, as shown in Fig. 1, the amplitude of the transfer function is more sensitive to τ_2 than the phase but τ_1 is a very sensitive predictor of the phase at high frequency. For the set of favored parameters, Fig. 6 shows the standard prediction and another with τ_2 set to 0.6 s instead, to show the sensitivity of this result to that parameter. The best prediction based on the measured phases consistently underestimates the ratio of spectra for frequencies below about 0.1 Hz and above about 3 Hz but is reasonably consistent with the observed ratio between 0.1 Hz and 3 Hz. Below 0.1 Hz it appears likely that the sensor is responding to real fluctuations in temperature not attributable to dynamic heating, as would be expected at these low frequencies. Above 3 Hz the prediction is much too low, probably because there is noise or other spurious variance in $T_m(t)$ not caused by dynamic heating.

The fit procedure used (7) and (8) to find the theoretical value of the amplitude ratio and phase at each frequency represented in the observations. For assumed values of the three parameters a, τ_1 and τ_2, a chi-square was calculated from the differences between these theoretical values and the observed values. The frequencies used for the fit were 0.01 to 12 Hz for the measurements of phase and 0.1 to 3 Hz for the measurements of amplitude ratio, to avoid regions where effects other than dynamic heating appear to bias the measurements. Then a search procedure varied these parameters to seek the minimum value of the chi-square.[7] The resulting values were $a = 0.73$, $\tau_1 = 0.031$ and $\tau_2 = 0.45$.

[7]The code can be found in the "Rnw" document that generates the present document. It used the

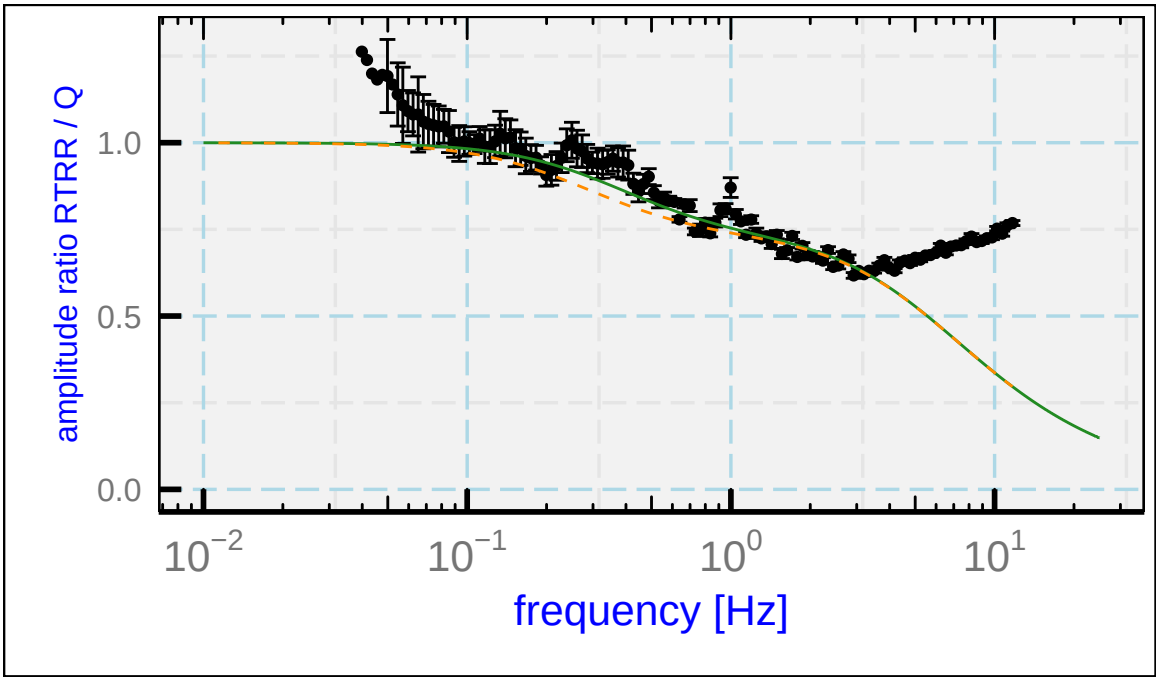

Figure 6: The ratio of the spectral amplitude for the measurement of recovery temperature ($T_m(t)$) to that for dynamic heating (Q), shown as the plotted data points. There are additional data points at frequencies below about 0.04 Hz that do not appear in this plot because they lie above the upper limit for the ordinate. The green line is the prediction from the transfer function determined from the best-fit values matching the phase lag between these variables, and the dashed orange line is a similar result with the second time constant τ_2 increased from 0.447 to 0.6 s to illustrate sensitivity to this parameter.

The chi-square for the fit is about 18 times larger than expected if the fit represents the measurements to measurement uncertainty, so it is difficult to assign uncertainty limits to this result on the basis of this fit because of this not-understood excess chi-square, but the fit minimum distinguished nearby values to about three significant digits in all three parameters. The Hessian from the fit implies that the results with standard uncertainties are $a = 0.733 \pm 0.004$, $\tau_1 = 0.0308 \pm 3 \times 10^{-4}$ and $\tau_2 = 0.45 \pm 0.02$.

To complete the cycle, the measured recovery temperature was then corrected via method 1 from Sect. 4.1, using these parameters, to find a prediction for the actual recovery temperature $T_r(t)$. After recalculating Q using (9) with that estimate of $T_r(t)$ in place of $T_m(t)$, the calculation of phase and amplitude was repeated and the results were fitted again by adjusting the fit parameters. Only very minor changes arose from this procedure even after one iteration, but the iterated result is the one used here to represent the unheated Rosemount 102E4AL sensor as flown in the NSF/NCAR C-130.

A similar evaluation examined the response of the same sensor when flown on the NSF/NCAR GV, which flies significantly faster than the C-130. The results of several studies using SOCRATES and CSET data were consistent with the results from VOCAL as used above,

"optim()" function from the R "stats" package produced by the R Core Team [2019].

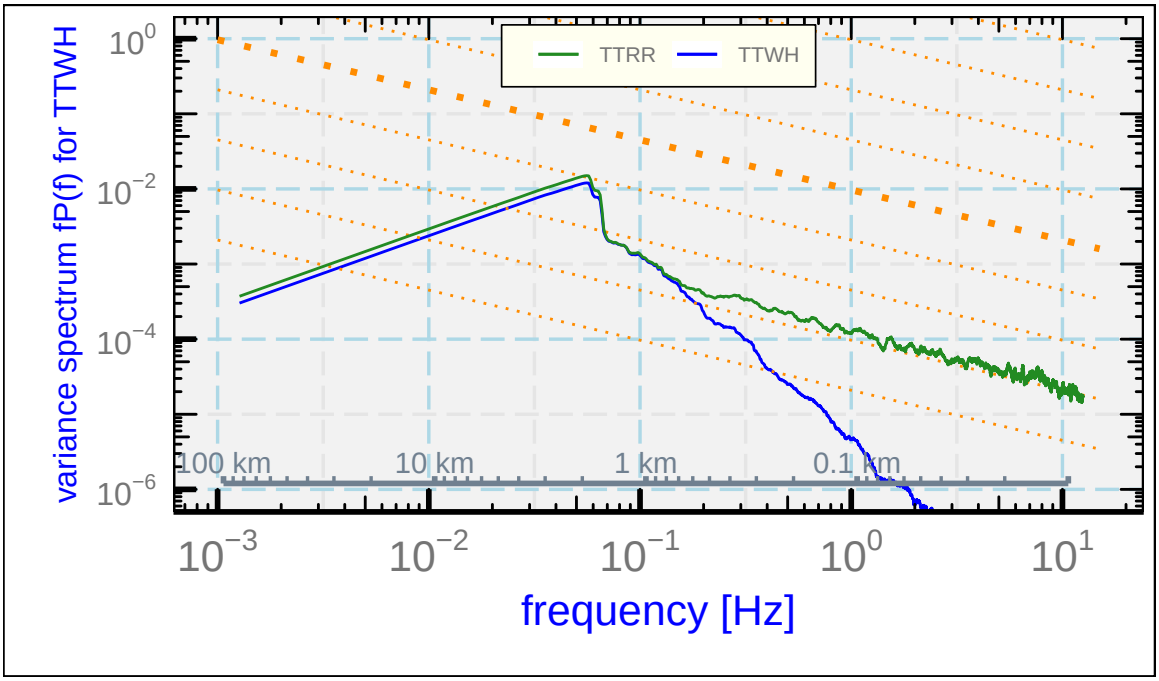

Figure 7: Variance spectrum for the recovery temperature measured by the heated Rosemount 102 sensor (TTWH) and by the unheated Rosemount sensor (TTRR).

in some cases with values of the two time constants τ_1 and τ_2 a little smaller than found for the C-130. This might be expected at greater airspeed, as discussed in Sect. 3.1.3.

3.1.2 The heated sensors

Measurements from two slower sensors, a heated Goodrich/Rosemount 102 sensor and a similar "Harco Model 100009-1 Deiced TAT" sensor, have also been evaluated. These sensors respond much more slowly than the unheated Rosemount and attempts to use the same three-parameter representation of the transfer function relative to dynamic heating led to unsatisfactory fits, so a different approach is used here. Because the evaluation in Sect. 3.1.1 provides a good representation of the unheated Rosemount 102E4AL sensor, the measurements from that sensor, corrected as described in Sect. 4, were used as the reference for the assumed-correct recovery temperature. Then the phase and amplitude ratio were found for the transfer function required to produce the heated-probe measurements from the unheated-probe measurement. This did not require any assumptions about equations or parameters determining the transfer function.

Measurements from the first five flight segments listed in Table 1 were used for characterization of the heated Rosemount 102 sensor. (The last segment was excluded because some of the measurements from the heated sensor were missing.) The spectral variance for the recovery-temperature measurement from the heated sensor has apparent rapid attenuation beginning at about 0.2 Hz, as shown in Fig. 7, and the response is attenuated seriously above about 1 Hz. The measured phase lag of the measurement behind

the measurement from the unheated Rosemount 102E4AL sensor is shown in the bottom panel of Fig. 8 and the corresponding estimate of the gain is shown in the top panel.

No combination of the three fit parameters $\{a,\ \tau_1,\ \tau_2\}$ entering the transfer-function equations (7) and (8) provides a satisfactory representation of the measurements in those two plots, although the best fit (shown as the "3-par" line) for the values {0.13, 0.47, 0.47} provides a fair approximation. Those figures show that the fit is inadequate (chisquare of over 16,000 for 40 degrees of freedom) so it appears that for this sensor heat transfer is still more complicated than can be represented by the differential equations (3) and (4), perhaps because there are other paths by which heat can be transferred to or from the sensing wire. The small value for the parameter a suggests that most of the heat transferred to or from the wire is through routes other than direct conduction from the air.

Rather than seeking a more complicated representation of the transfer function, it can be represented instead by the lines in Fig. 8 labeled "lfit", fits to the measurements in terms of $x = \log_e(\nu/\nu_0)$ where $\nu = \omega/(2\pi)$ is the frequency and $\nu_0 = 1\,\mathrm{Hz}$:

$$\text{for } \nu > 0.08\,\mathrm{Hz},\ H(\omega) = (h_0 + h_1 x + h_2 x^3 + h_3 x^5 + h_3 \arctan(\nu/\nu_0))e^{i\phi(\omega)} \tag{12}$$

$$\text{for } \nu \le 0.08\,\mathrm{Hz}, \quad H(\omega) = 1$$

$$\phi(\omega) = p_0 + p_1 x + p_2 x^2 + p_3 \arctan(\nu/\nu_0)$$

The coefficients obtained by fitting to the observations are h_{0-3} ={0.138, −0.209, −0.0695, 0.00747} and p_{0-3} ={−239.2, −113.0, −13.40, 138.6}. These equations are the basis for the "lfit" lines plotted in Fig. 8. The reason that the three-parameter fit is unacceptable is that there is conflict between the constraints imposed by the amplitude ratio and the phase, such that either could be represented reasonably but not both. The actual transfer function has some complex features, including frequencies where the phase shift reaches values below −90° (not possible for a simple exponential time response) and values of the phase shift of about −36° at 0.1 Hz where the amplitude ratio remains near unity. The amplitude decreases to e^{-1} at about 0.4 Hz, as would be the case for a first-order time constant of about 1 s, so this could be considered another measure of the response. However, that value does not extrapolate well to other frequencies and the phase shift at 0.4 Hz is approximately −90°, which would indicate that the measurement of a real contribution to sensible-heat flux at this frequency would be zero.

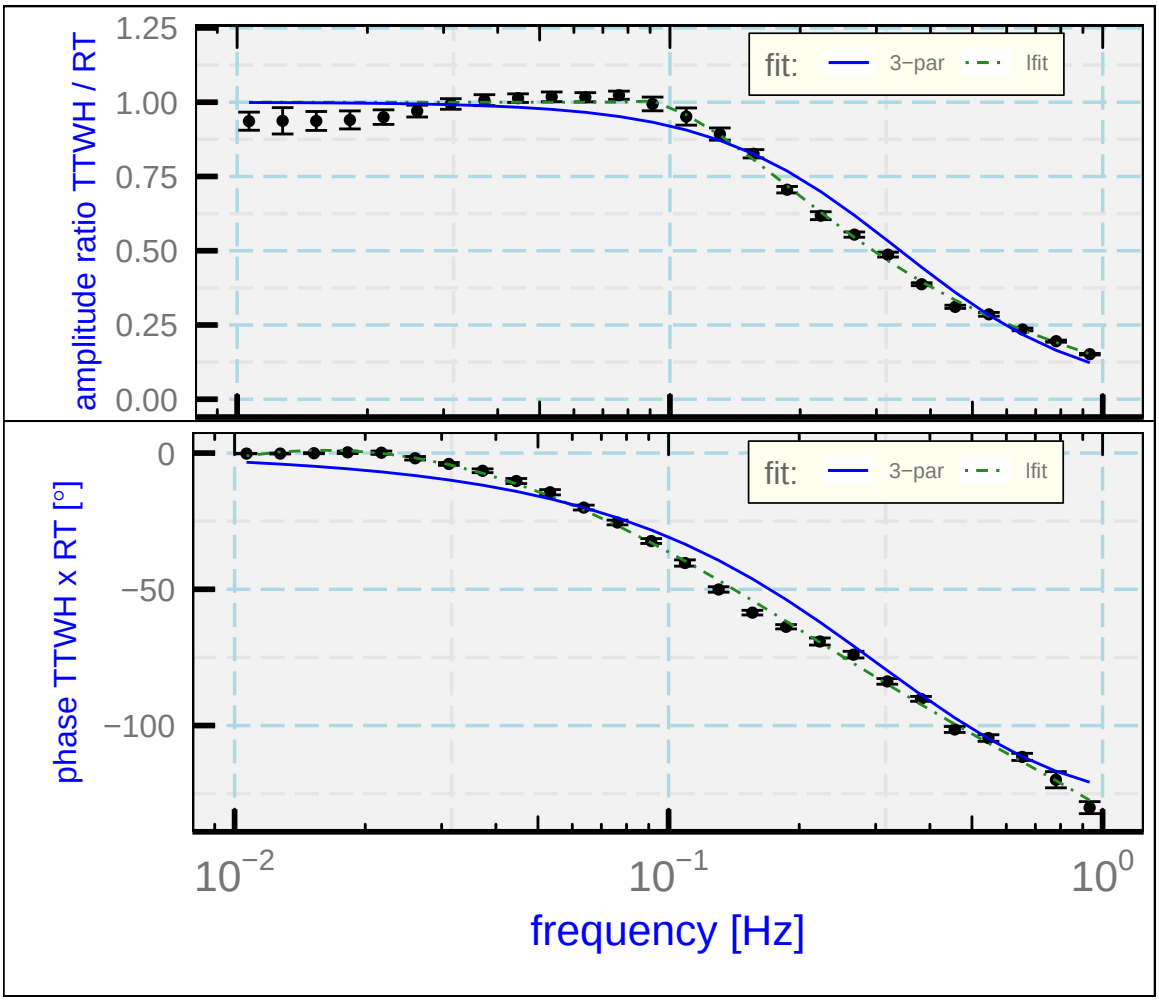

Figure 8: The gain (top) and phase (bottom) of the transfer function determined for the heated Rosemount 102 sensor (variable TTWH) and the recovery temperature obtained by applying transfer-function corrections to the measurments from the unheated Rosemount 102E4AL sensor (variable RT). Error bars are two-standard-deviation estimates of the uncertainty in the mean values shown by plotted circles. Because the results showed high variability and inconsistency for frequencies above 1 Hz, only results for frequencies below that limit are shown. The fits are described in the text.

The heated HARCO sensor was not flown on the same flights used to study the heated Rosemount 102 sensor, so flight segments from the SOCRATES and CSET projects, listed in Table 2, were used for the HARCO sensor.

Project/Flight	**start [UTC]**	**end[UTC]**
CSET/rf05	2015-07-14 17:52:00	18:02:00
CSET/rf05	2015-07-14 19:45:30	19:55:30
CSET/rf05	2015-07-14 20:37:17	20:47:17
SOCRATES/rf15	2018-02-24 5:52:00	6:02:00
SOCRATES/rf15	2018-02-24 6:05:00	6:15:00

Table 2: Flight segments used to determine the response characteristics of a heated HARCO sensor.

Flight segments were all at low level and in boundary-layer conditions and were of equal duration to facilitate averaging of the variance spectra. The measured phase and amplitude ratio for this data set are shown in Figs. 9. The best fit for the response function defined by (7) and (8) is shown as the blue line labeled "3-par" in that figure. The best-fit values for $\{a, \tau_1, \tau_2\}$ were $\{0, 0.05, 1.12\}$, and to obtain this result the fit had to be constrained to keep a non-negative. A value of zero for the parameter a would indicate that no heat is transferred from the sensing wire to the air, but instead all is transferred to the support which has a relatively slow characteristic response. The transfer function is quite similar to that of the heated Rosemount 102 sensor shown in Fig. 8, and the typical variance spectrum shows a decrease with frequency similar to that in Fig. 7.

As for the heated Rosemount, the best fit is not consistent with the measurement errors even though it provides an approximate representation of the transfer function. Therefore fits in the logarithm of the frequency were again used to provide a better representation of the measurements, as shown by the dashed green lines labeled "lfit". Those fits are given by these equations and coefficients: with $x = \log_e(\nu/\nu_0)$ where $\nu = \omega/(2\pi)$ is the frequency and $\nu_0 = 1\,\text{Hz}$:

$$\text{for } \nu > 0.024\,\text{Hz},\ H(\omega) = (h_0 + h_1 x + h_2 x^3 + h_3 x^4 + h_4 x^5) e^{i\phi(\omega)} \tag{13}$$

$$\text{for } \nu \le 0.024\,\text{Hz}, \quad H(\omega) = 1$$

$$\phi(\omega) = p_0 + p_1 x + p_2 x^2 + p_3 \arctan(\nu/\nu_0)$$

The coefficients obtained by fitting to the observations are h_{0-4} ={0.161, −0.136, −0.0760, −0.0309, −0.00324} and p_{0-3} ={−155.2, −62.8, −6.35, 67.2}.

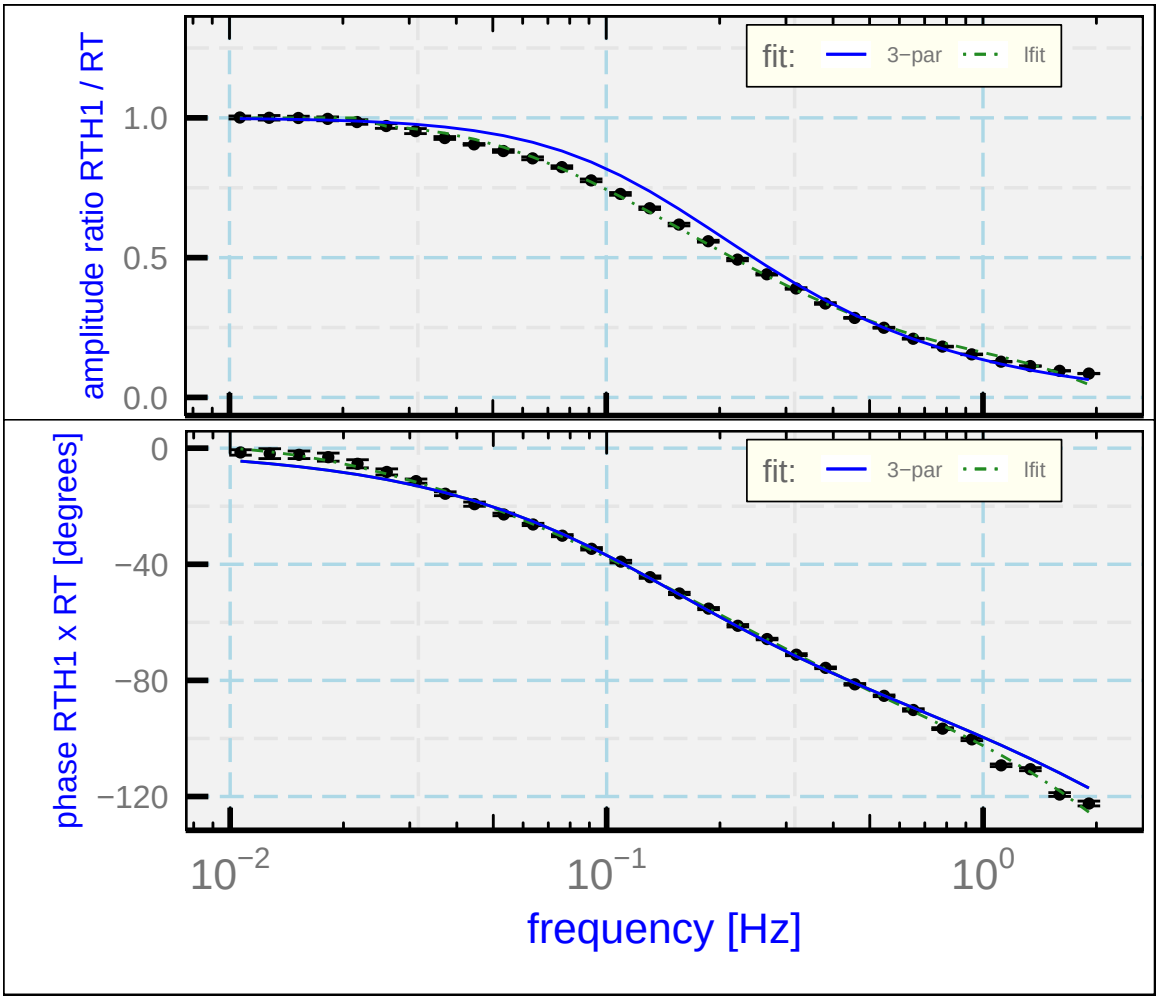

Figure 9: The gain (top) and phase (bottom) for the transfer function characterizing a heated HARCO temperature sensor. The measurements are indicated by error bars that show two-standard-deviation limits from the mean value). Two fits to the measurements, one based on the three-parameter representation and one on a polynomial fit, are described in the text.

3.1.3 Expected dependence on flight conditions

Based on measurements in a wind tunnel, Stickney et al. [1994] indicated that the fast-response characteristic time τ_1 for the unheated Rosemount 102E4AL sensor varies approximately as $\log(Z^{-0.6})$ where $Z = M\rho_a/\rho_s$ with M the Mach number, ρ_a the air density and ρ_0 the air density under standard conditions. The mean value of Z for the flight segments used to find the best-fit parameters was $Z = 0.3$, so this suggests that the first characteristic time for that sensor is best represented by

$$\tau_1'(Z) = \tau_1 \left(\frac{0.3}{Z} \right)^{0.6} \quad . \tag{14}$$

For GV flight conditions, Z can vary from about 0.18 to 0.38, so this suggests a range for τ_1 from 0.029 to 0.046 s. There is no similar evidence for τ_2, but it might be expected to have similar dependence because this is approximately the Reynolds number dependence and the Nusselt number characterizing ventilated heat transfer often is represented by a power-law relationship to the Reynolds number. If both heat transfer terms scale similarly, it might be expected that a will be unchanged.

For these reasons, the time parameters obtained in preceding sections have been adjusted to a reference value of $Z = 0.3$ in the Table 3. For other conditions, it is suggested that the best estimate will be to multiply τ_1 and τ_2 by $(0.3/Z)^{0.6}$.

sensor	a	τ_1 [s]	τ_2 [s]
unheated Rosemount 102E4ALon C-130	0.73	0.031	0.45
unheated Rosemount 102E4AL on GV	0.65	0.024	0.22
heated Rosemount 102 on C-130	0.13	0.47	0.47
heated HARCO on GV	0.0	0.057	1.25

Table 3: Parameters for the time response of available temperature sensors on the NSF/NCAR aircraft, adjusted to $Z = 0.3$. For other conditions, scale as represented for τ_1' in (14).

3.2 Response to a step change

The preceding subsection developed estimates of the response parameters for various sensors with low uncertainty compared to previous estimates, so that will be the primary constraint on these parameters. It is nevertheless useful to investigate other measurements that can constrain the response parameters. Previous studies have mostly used sharp temperature changes in the atmosphere, for example from climbs through the inversion at the top of a boundary layer, to study the time response. A search of representative VOCALS climbs and descents through inversions capping the marine boundary layer

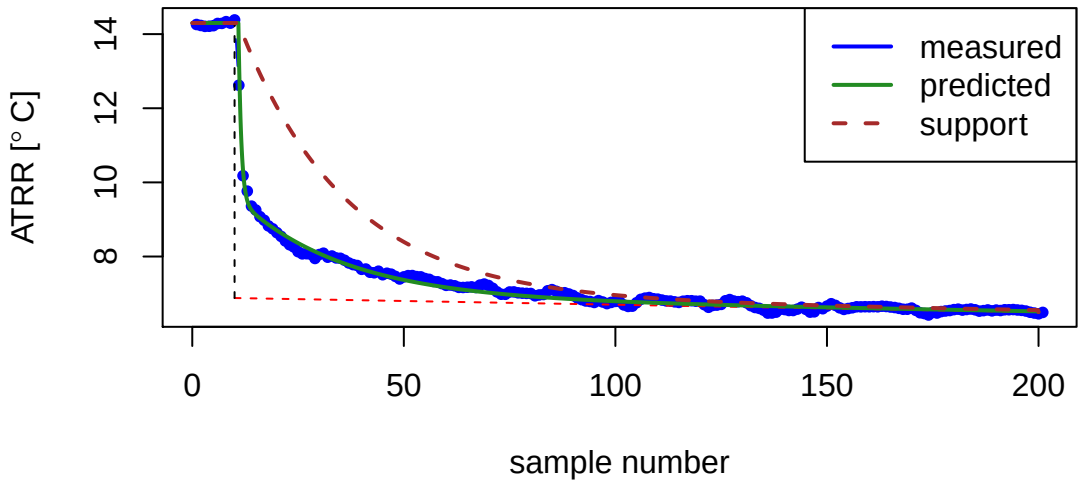

Figure 10: (blue dots): Temperature measured at 25 Hz during descent through an inversion capping the marine boundary layer, from VOCALS flight 3, starting at 8:13:50 UTC. The descent rate was approximately 5 m/s. The dashed red line shows a dry-adiabatic lapse rate in the marine boundary layer, and the dashed black line is a reference line indicating the location of the top of the boundary layer.The prediction using the parameters listed in the text is shown as the green line, significantly obscured by the blue dots representing the measurements. The dashed brown line is the calculated temperature of the support that contacts the sensing wire.

found many with unusable structure but one near-ideal example, from VOCALS research flight 3, with a descent through the inversion at 8:13:50 UTC. The instrument list for this experiment includes two unheated Rosemount102E4AL sensors, including ATRR (ATX). Figure 10 shows the time history of the measured temperature for 8 s during this descent, at a rate of approximately 1000 ft/min (around 5 m/s). The temperature structure in this case is remarkably consistent with a near-constant temperature above the inversion and a near-adiabatic-temperature structure below the inversion.

The suggested measurand history, if the discontinuity at the inversion is discrete, is that shown by the dashed black and dashed red lines, x(t)={14.3, 6.878, 6.876, 6.874, 6.872, 6.870, 6.868, 6.866, 6.864, 6.862, 6.860, ...} for t={10, 11, 12, ...}. The predicted time response from (4) for assumed time constants for the unheated Rosemount 102E4AL sensor adjusted for air density and flight speed is shown as the green line in Fig. 10. The predicted response is consistent with the observations and supports the validity of the parameters determined from fits to the response to dynamic heating.

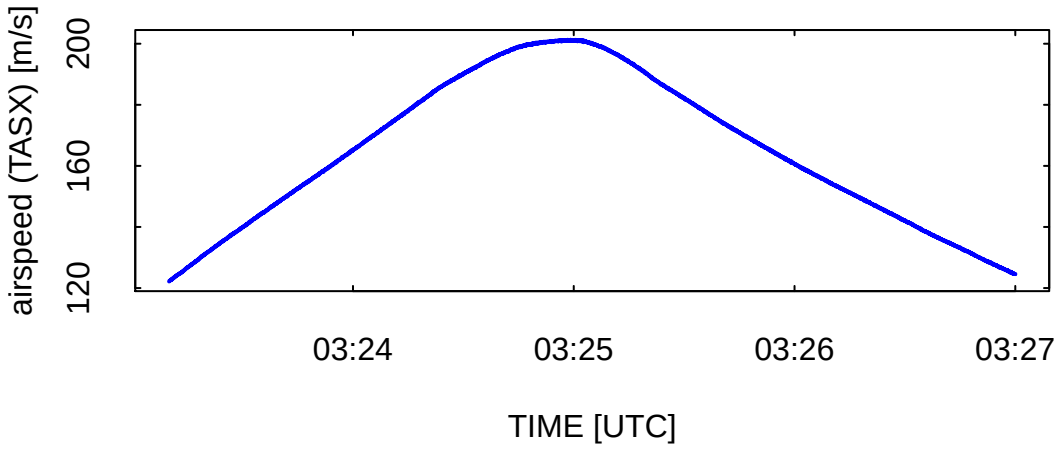

Figure 11: History of the airspeed during a segment of flight 15 from the DEEPWAVE project (a "speed-run" maneuver).

3.3 Application to a speed run

Because the assumed response of the support is characterized by a simple time constant, during the speed run the support will lag in temperature by τ_2. Then, from (4), $T_m(t)$ will lag by τ_1 behind the temperature to which the sensor responds, which is $aT(t) + (1-a)T(t-\tau_2)$. For a ramp input such that $T(t) = T_0 + kt$, the solution to (4) is that the measured temperature $T_m(t)$ lags $T(t)$ by ψ, so that $T_m(t) = T_0 + k(t-\psi)$. Then

$$k\tau_1 = a(T_0 + kt) + (1-a)(T_0 + k(t-\tau_2) - T_0 - kt + k\psi$$

which requires the recovery-temperature lag to be

$$\psi = \tau_1 + (1-a)\tau_2 \tag{15}$$

For the Rosemount 102E4AL, the fitted values from Sect. 3.1.1 would then cause a lag of 0.15 s. For the heated HARCO probe the predicted lag would be 1.31 s.

An example of a speed run is shown in Fig. 11, where the airspeed was increased steadily in level flight from near the lower limit of the flight envelope to near the upper limit and then was decreased back to the starting value. A plot of recovery temperature should also increase and decrease with a lag given by (15). For a HARCO heated sensor, this plot is shown in Fig. 12. The hysteresis depicted by the difference between the segment with increasing speed and that with decreasing speed arises from the sensor time lag. Because the Mach number and hence the time parameters vary significantly during the speed run, a test of the time-response parameters is to apply the first correction scheme outlined in

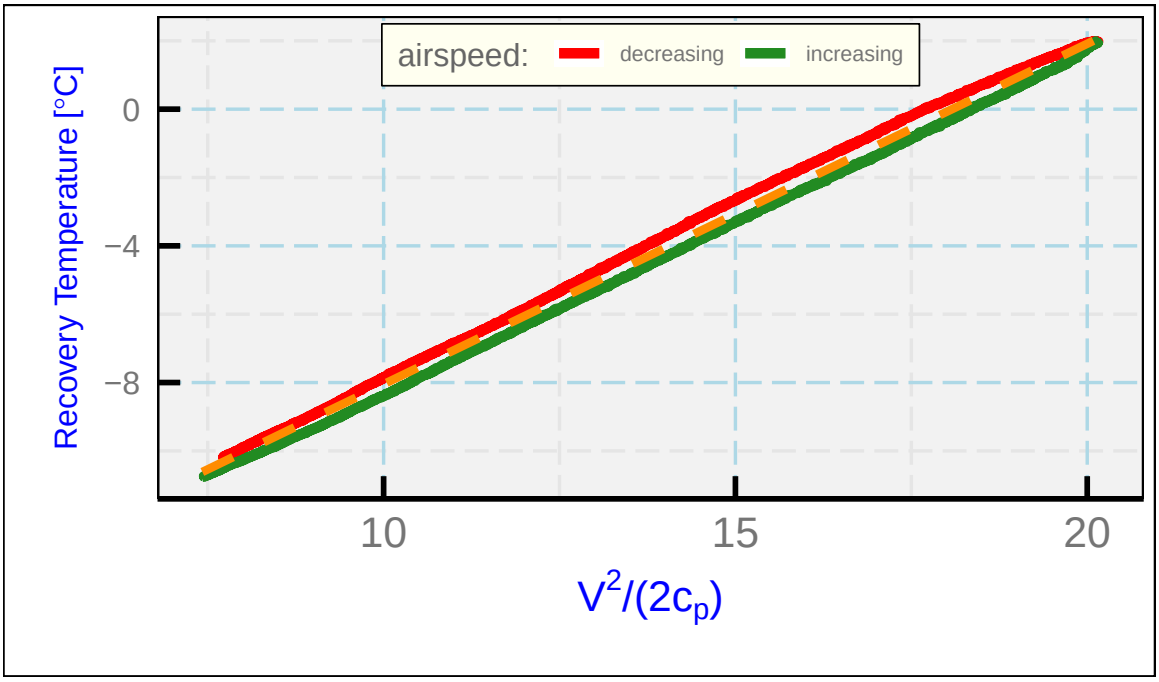

Figure 12: The recovery temperature measured during the speed-run maneuver shown in the previous figure, without any imposed delay. The dashed orange line indicates the regression fit, with standard deviation about the fit of 0.26°C.

Sect. 2.2 to the measurements. For $a = 0$, as for the heated HARCO, the solution for the estimated actual recovery temperature $T_r(t)$ is

$$T_r(t) = (\tau_1 + \tau_2)\frac{dT_m(t)}{dt} + T_m(t) + \tau_2\tau_1\frac{d^2T_m(t)}{dt^2} \tag{16}$$

No integration is needed because all terms on the right side are measured or obtainable from finite differences. This is particularly suited to the speed run because the variation in τ_1 and τ_2 with airspeed can be incorporated into the solution. Figure 13 shows that the delay is mostly removed by this procedure. The residual standard deviation about the fit is reduced from 0.26°C before correction to 0.12°C after correction. The minimum standard deviation results from increasing the time constants by 12%, so measurements from this speed-run maneuver indicate that the time response determined for the heated HARCO sensor is valid to within about this uncertainty.

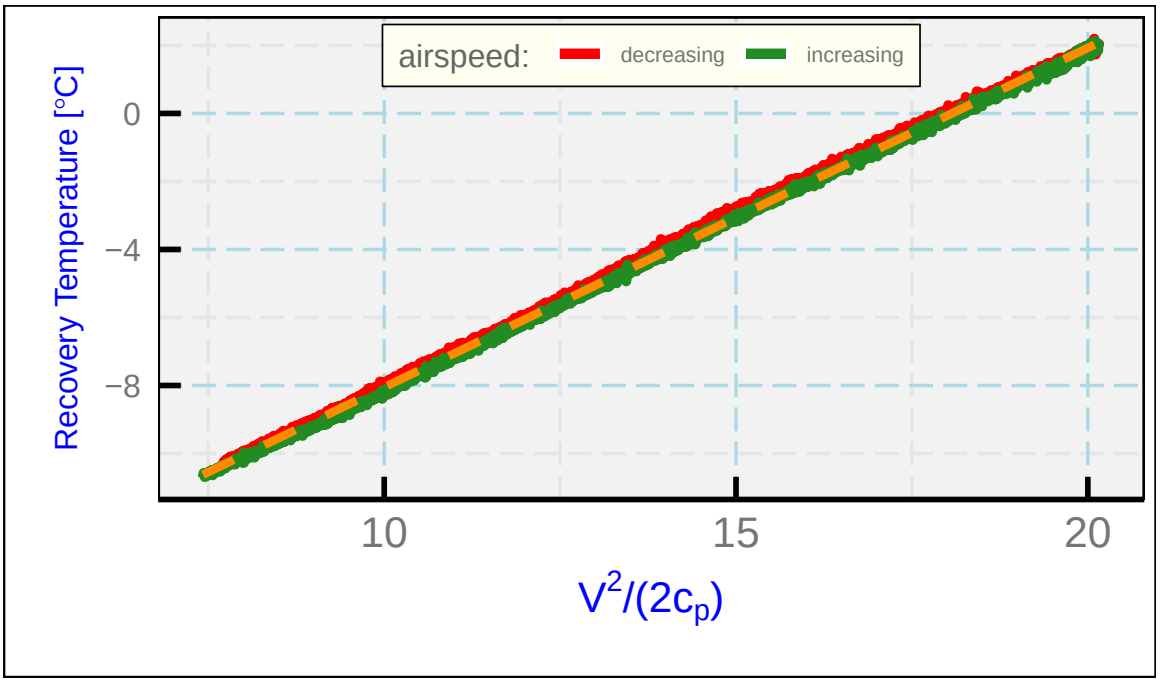

Figure 13: The same measurements as shown in the previous figure but with the measurements of recovery temperature corrected to compensate for the response time of the heated HARCO sensor. The residual standard deviation about the fit is $0.12^{\circ}C$ *after this correction.*

4 Correcting the Temperature

The true recovery temperature T_r can be retrieved from the measured temperature T_m in two ways, either from the differential equations or by Fourier transformation. These methods are illustrated here.

4.1 Integration of the differential equations

The differential equations (3) and (4) provide a basis for correcting the measured temperature to account for the time response of the sensor. They should be applied to the recovery temperature $T_r(t)$, which is the measurand. The actual measurement is $T_m(t)$ and the temperature of the support is $T_s(t)$, so those equations, rearranged, are:

$$\frac{dT_s(t)}{dt} = \frac{T_r(t) - T_s(t)}{\tau_2} \tag{17}$$

$$T_r(t) = \frac{1}{a}\left\{\tau_1 \frac{dT_m(t)}{dt} + T_m(T) - (1-a)T_s(t)\right\} \tag{18}$$

There are two unknowns ($T_r(t)$, the actual recovery temperature, and $T_s(t)$). Those unknowns are specified by the two preceding equations because all other terms are known, including dT_m/dt which can be represented using the numerical derivative of the measurements $T_m(t)$. The second equation can be used to eliminate T_r from the first:

$$\frac{dT_s(t)}{dt} = \frac{\frac{1}{a}\left\{\tau_1 \frac{dT_m(t)}{dt} + T_m(T) - (1-a)T_s(t)\right\} - T_s(t)}{\tau_2} \tag{19}$$

From an initial value $T_s(0)$, assumed to be $T_m(0)$, this equation can be integrated to find the temperature of the support, $T_s(t)$. Once that is known, (18) specifies the estimate of the true recovery temperature $T_r(t)$ without further integration. The only choices needed are the numerical method used to find the derivative dT_m/dt (e.g., here from consecutive differences or higher-order approximations) and the integration method applied to (19), here a fourth-order Runge-Kutta integration with Cash-Karp Cash and Karp [1990] adjustment of the step size.

The HARCO presents a special case because the best-fit value is $a = 0$ so (18) can't be used. However, in this case the differential equations can still be combined to give

$$T_r(t) = (\tau_1 + \tau_2)\frac{dT_m(t)}{dt} + T_m(t) + \tau_2\tau_1\frac{d^2T_m(t)}{dt^2} \tag{20}$$

a form that can be used directly without integration because finite-difference equations can be used for the derivatives of the measured $T_m(t)$. However, this is not as good a representation of the transfer function as is possible with the fitted representation shown in Fig. 9 and given by (13). That fit can be used with the Fourier-transform approach to correction, as shown in the next subsection.

An example of the corrected recovery temperature will be shown in the next subsection, where the two approaches to correction can be compared.

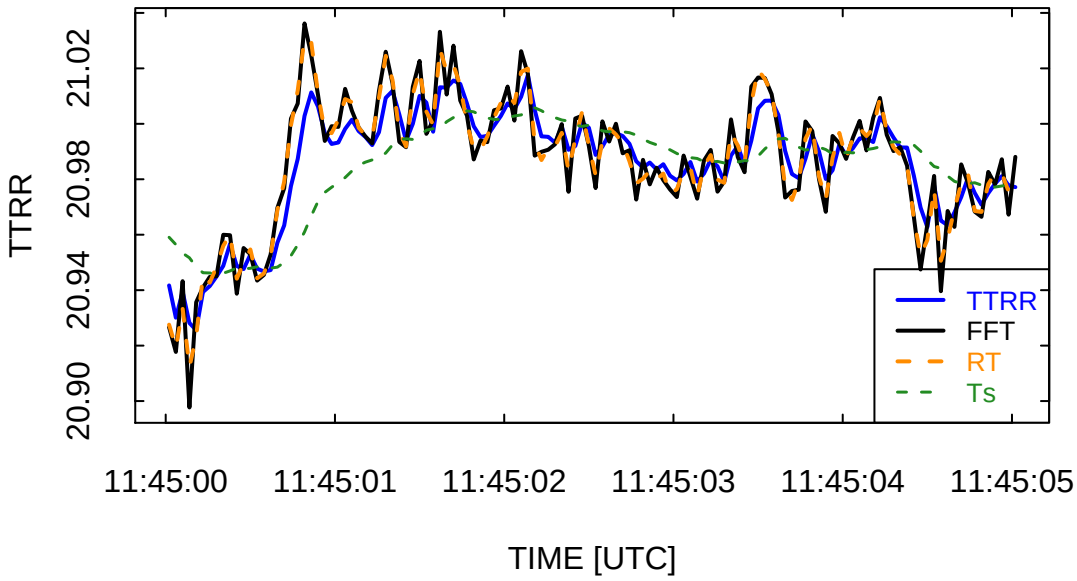

Figure 14: Example of the change produced by the FFT correction procedure. The original measurement of recovery temperature is TTRR and the revised value is FFT. The corrected value obtained by the previous method (RT) is also shown. The dashed green line labeled "Ts" is the calculated temperature of the support. The plotted time is seconds after 11:45:00 UTC for VOCALS flight 3.

4.2 Inverse Fourier transformation

An alternate approach is to use Fourier transforms:

1. Calculate the Fourier transform of the measured time series: $M(\omega) = \mathcal{F}(T_m(t))$ where ω is the angular frequency and $\mathcal{F}$ denotes the Fourier transform.

2. Divide the result by the complex representation of the transfer function: $X(\omega) = M(\omega)/H(\omega)$. If the Fourier transform covers positive and negative frequencies, so should the transfer function.

3. Use the inverse Fourier transform to find a retrieved estimate of the recovery temperature: $T_r(t) = \mathrm{Re}\left(\mathcal{F}^{-1}(X(\omega))\right)$ where Re denotes the real part of the complex result.

The result of this procedure is illustrated in Fig. 14, where the result is shown along with that obtained by the preceding method. The agreement between the two correction methods is very good, and both show evidence of faster and higher-amplitude response

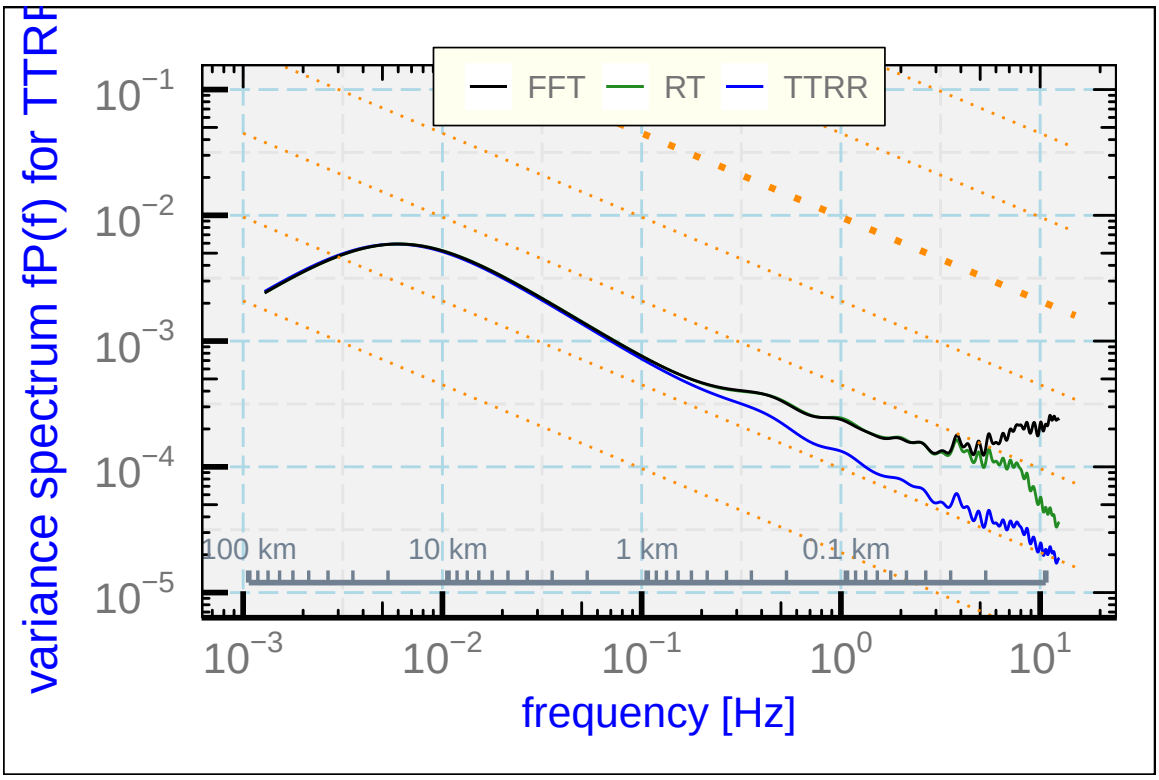

Figure 15: Variance spectra for the original measurement of recovery temperature (TTRR) and for the corrected value (FFT).

to fluctuations. The Foureir-transform method provides some higher-amplitude changes and may be preferable. However, the resulting variance spectrum (Fig. 15) appears less satisfactory because it has high variance above about 5 Hz that is not understood. This is likely the fault of the measurement itself, although the correction procedure tends to amplify whatever causes this excess noise.

Taking the Fourier transform of an entire 25-Hz measurement for a flight of several hours becomes impractical. However, it is possible to segment the time series, calculate Fourier transforms for the segments, and then combine the results to represent the entire flight. Tests have shown that, for example, dividing into 2^{16}-sample overlapping segments, using fast Fourier transforms, and combining the middle half of each segment is feasible with many-hour flights and 25-Hz data.

4.3 Application to the HARCO sensor

Because the heated HARCO sensor is much slower than the unheated Rosemount 102E4AL sensor, the measurements from that slower sensor can't be corrected to the extent possible for the unheated sensor, but it is still useful to evaluate to what extent the measurements can be improved. The most straightforward correction is to apply (20), even though that is based on an inferior representation of the transfer function in comparison to (13). The solution from (20) is very noisy if first-order finite-difference estimates of the derivatives are used, so some smoothing of the result was needed. Figure 16 shows the result (as "RTHC, the dash-dot orange line) where a Butterworth low-pass filter with cutoff frequency of 2 Hz has smoothed the corrected measurements from a heated HARCO sensor. In comparison to the original measurement (labeled "RTH1"), the response of the sensor is greatly improved by this correction procedure and it even provides a reasonable representation of the best measurement (labeled "RT").

Alternately, the transfer function was calculated from (13) and the Fourier transform of the measured sequence was divided by this transfer function to obtain the Fourier transform of the corrected measurement. The result is shown in Fig. 16 as the black line labeled "RTFFT". This is also a significant improvement over the original and reproduces many of the features of the best measurement ("RT"), but it appears to respond less quickly to changes in that reference measurement. To obtain this result, it was necessary to attenuate frequencies above 1 Hz in the Fourier transform representing the corrected measurement because there is a zero in the transfer function that otherwise invalidates the inversion. This attenuation was accomplished by multiplying the transfer function by $e^{3\nu}$above 1 Hz after setting values with modulus smaller than 0.05 to 1. This arbitrarily chosen attenuation gave reasonable results, although it is likely that better choices could be made with further exploration. One more general measure of the improvement, beyond the anecdotal evidence in that figure, is that either correction procedure reduced the standard deviation of the difference between the measured value (RTH1) and the estimated best value (RT) from 0.06°C before correction to 0.03°C after correction.

The plot of variance spectra (Fig. 17) shows that the original spectrum (orange line labeled "RTH1" is seriously attenuated at high frequencies relative to the reference measurement

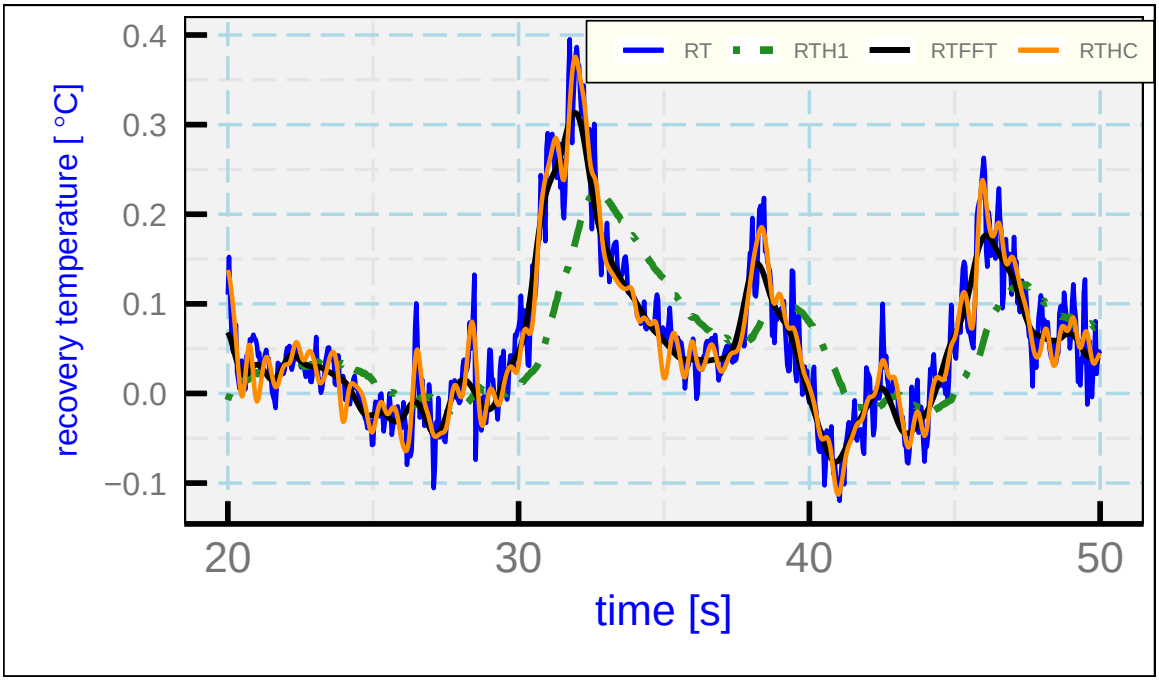

Figure 16: Corrected recovery temperature as measured by a heated HARCO sensor ("RTHC" and "RTFFT"), the uncorrected measurement ("RTH1"), and the best estimate of the true recovery temperature ("RT") based on an unheated Rosemount sensor after correction. The time is seconds after 2018-02-24 5:59:00 UTC, SOCRATES flight 15. "RTHC" is based on the approximate formula (20), while "RTFFT" results from Fourier transformation after correction using the transfer function determined from (13). Mean values have been subtracted from all to facilitate comparisons.

("RT") and that both correction procedures restore significant parts of the missing spectral variance and increase the apparent cutoff frequency to 1 Hz or, in the case of the first method, almost 2 Hz. It does not appear possible to restore the missing high-frequency fluctuations (above about 1 or 2 Hz) because the original measurement is so severely attenuated at these frequencies. This sensor and the similar heated Rosemount sensor are therefore unable to detect contributions to sensible-heat flux from this frequency range, even after corrections. It nevertheless appears useful to apply one of these correction approaches routinely to improve the quality of the measurements.

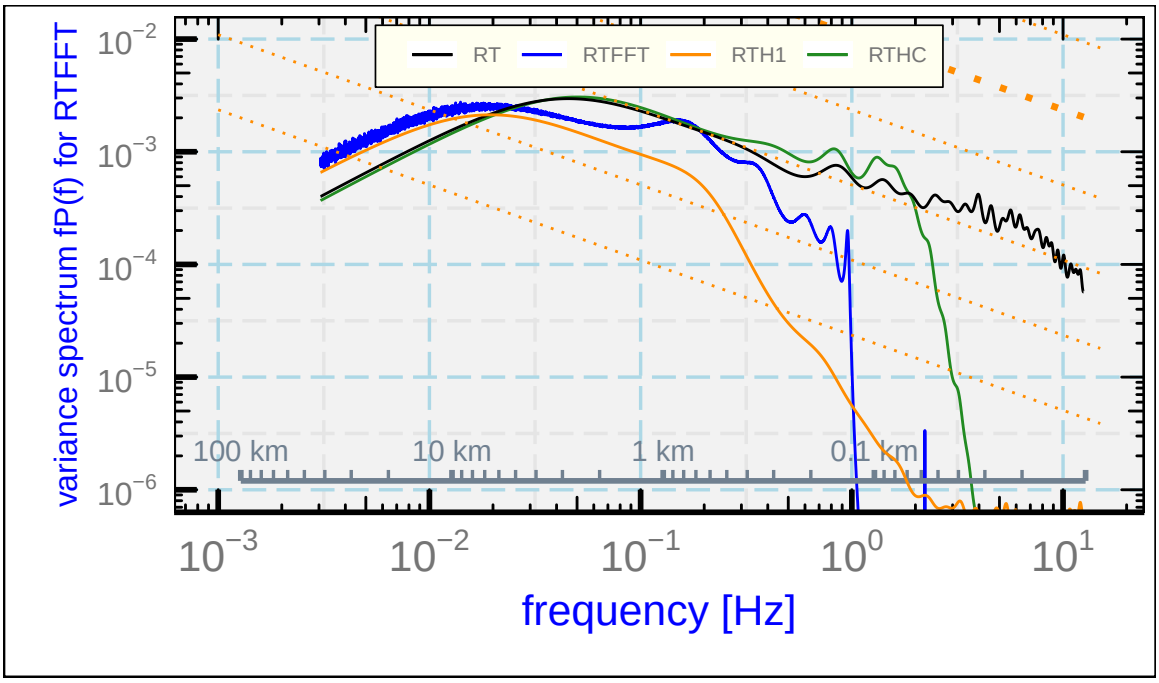

Figure 17: Variance spectra for some measurements of recovery temperature: "RT" (the best estimate resulting from correction of the measurements from the unheated Rosemount 102E4AL); "RTH1" (the uncorrected measurement from the heated HARCO); "RTFFT" (the corrected HARCO measurement based on Fourier transforms); and "RTHC" (the corrected HARCO measurement based on the correction formula (20)).

5 Summary and Conclusions

Findings and conclusions of this investigation include these items:

1. The differential equations (3) and (4), with appropriate parameters, provide an analytical representation of the transfer function for the recovery temperature measured by an unheated Rosemount 102E4AL sensor. That transfer function was shown to be consistent with measurements of the phase and amplitude ratio of the response to dynamic-heating fluctuations. This is good evidence that the equations provide a good representation of the time response for that sensor, although the consistency with the predictions of the equations is less satisfactory when applied to the heated HARCO sensor or the heated Rosemount sensor.

2. The three parameters in those equations, characterizing the two time constants and the fraction of heat transfer to the air vs. that to the structure supporting the sensing wire, can be determined with small uncertainty by fitting the transfer function while varying those parameters to observations of dynamic heating. These parameters are thus constrained well and can be relied upon to make corrections to the measurements and otherwise to characterize the effects of time response of the sensors.

3. Once the transfer function for the unheated Rosemount sensor has been determined, it can be used to estimate the true recovery temperature, and then transfer functions for other sensors can be determined by comparison to that estimate of the measurand to which they are responding.

4. Some additional evidence, esp. from measurements during passage through sharp features in the atmosphere or during "speed runs" when the aircraft flies at varying speed at constant altitude, support the general magnitude of the parameters.

5. Two correction schemes are suggested and verified, one based on integrating the derivatives provided by the differential equations and one based on taking the Fourier transform of the time series, correcting that transform as indicated by the transfer function, and then recovering the original signal from the inverse Fourier transform. Both could be used for routine processing to correct for the response characteristics of airborne temperature sensors.

This Part-I paper has focused on the measured temperature, the "recovery" temperature. Part II will consider how these results affect calculation of the actual air or ambient temperature, which requires subtraction of the contribution from dynamic heating. It will be argued there that the temperature sensor cannot respond to the rapid fluctuations in dynamic heating often present in a turbulent atmosphere, and therefore conventional data processing introduces errors by trying to compensate for fluctuations that do not appear in the measured recovery temperature. Because this error is so prevalent in almost all existing data from research aircraft, it is essential to determine how to remove these errors. Once this problem is addressed, Part III will then turn to the implications for measuring the flux of sensible heat.

A Reproducibility

This document is constructed in ways that support duplication of the study. The code that generates the plots and implements the correction procedure is incorporated into the same file that generated this document via LaTeX, using principles and techniques described by Xie [2013] as implemented in the R package 'knitr' (Xie [2014]). The program, 'SensibleHeatFluxPaper1.Rnw', is archived on 'GitHub' in the directory at this URL. There is some supplemental material in that directory, including the workflow document, the bibliography and some code segments saved in the "chunks" subdirectory, so the full directory should be downloaded in order to run the program. The calculations use the programming language R (R Core Team [2019]) and were run within RStudio (RStudio [2009]), so this is the most straightforward way to replicate the calculations and the generation of this document.

A package named Ranadu, containing auxillary functions, is used extensively in the R code. It is available on GitHub as https://github.com/WilliamCooper/Ranadu.git. The version used for calculations in this technical note is included in the 'zip' archive listed below.

The data files used are also preserved in the NCAR/EOL Data Archives and can be obtained via a request to `mailto:raf-dm@eol.ucar.edu` or via the "Data Access" links at this web site. The original files containing the data as produced by the NCAR Earth Observing Laboratory, Research Aviation Facility, were in netCDF format (cf. this URL), but in many cases data archives were reprocessed and the files may change after reprocessing so a separate archive is maintained for this document. The data files in this archive contain R data.frames and are preserved as binary-format 'Rdata' files via R 'save' commands. The code in the GitHub archive has appropriate 'load' commands to read these data files from a subdirectory named 'Data' (/Data or ~/Data or /home/Data) but this is not part of the GitHub repository because it is too large to be appropriate there. To reproduce this research, those data files have to be transferred separately from {??where??}

Extensive use has been made of attributes assigned to the data.frames and the variables in those data.frames. All the attributes from the original netCDF files have been transferred, so there is a record of how the original data were processed, for example recording calibration coefficients and processing chains for the variables. Once the data.frames are loaded into R, these attributes can be viewed and provide additional documentation of what data were used. Key information like the processing date, the program version that produced the archive, and the selection of primary variables for various measurements thus is preserved.

(See the related list of project components on the next page that are preserved to enhance reproducibility.)

PROJECT:	SensibleHeatFlux
ARCHIVE PACKAGE:	SensibleHeatFluxPaper1.zip
CONTAINS:	attachment list below
PROGRAM:	SensibleHeatFluxPaper1.Rnw
ORIGINAL DATA:	UCAR/NCAR - Earth Observing Laboratory [2011],UCAR/NCAR - Ea
SPECIAL DATA FILES:	SensibleHeatFluxTechNote.Rdata, SensibleHeatFluxTechNote2.Rdata
WORKFLOW DOCUMENT:	WorkflowSensibleHeatFluxPaper1.pdf
GIT:	https://github.com/WilliamCooper/SensibleHeatFlux.git

Attachments:
SensibleHeatFluxPaper1.Rnw
SensibleHeatFluxPaper1.pdf
WorkflowSensibleHeatFluxPaper1.pdf
WAC.bib
chunks/*
SessionInfo

References

Jens Bange, Marco Esposito, Donald H. Lenschow, Philip R. A. Brown, Volker Dreiling, Andreas Giez, Larry Mahrt, Szymon P. Malinowski, Alfred R. Rodi, Raymond A. Shaw, Holger Siebert, Herman Smit, and Martin Zöger. *Measurement of Aircraft State and Thermodynamic and Dynamic Variables*, chapter 2, pages 7–75. John Wiley & Sons, Ltd, 2013. ISBN 9783527653218. doi: 10.1002/9783527653218.ch2. URL https://onlinelibrary.wiley.com/doi/abs/10.1002/9783527653218.ch2. 3.1.1

Jeff R Cash and Alan H Karp. A variable order runge-kutta method for initial value problems with rapidly varying right-hand sides. *ACM Transactions on Mathematical Software (TOMS)*, 16(3):201–222, 1990. 4.1

W. A. Cooper, S. M. Spuler, M. Spowart, D. H. Lenschow, and R. B. Friesen. Calibrating airborne measurements of airspeed, pressure and temperature using a doppler laser air-motion sensor. *Atmospheric Measurement Techniques*, 7(9):3215–3231, 2014. doi: 10.5194/amt-7-3215-2014. URL http://www.atmos-meas-tech.net/7/3215/2014/. 1.1

W. A. Cooper, R. B. Friesen, M. Hayman, J. B. Jensen, D. H. Lenschow, P. A. Romashkin, A. J. Schanot, S. M. Spuler, J. L. Stith, and C. Wolff. Characterization of uncertainty in measurements of wind from the NSF/NCAR Gulfstream V research aircraft. NCAR technical note NCAR/TN-528+STR, Earth Observing Laboratory, NCAR, Boulder, CO, USA, jul 2016. URL http://n2t.net/ark:/85065/d7qr4zqr. 1.1

C. A. Friehe and D. Khelif. Fast-response aircraft temperature sensors. *J. Atmos. Ocean. Technol.*, 9(6):784–795, DEC 1992. ISSN 0739-0572. doi: 10.1175/1520-0426(1992)009<0784:FRATS>2.0.CO;2. 1.1, 1.1, 2.1

Berend Hasselman. *nleqslv: Solve Systems of Nonlinear Equations*, 2018. URL https://CRAN.R-project.org/package=nleqslv. R package version 3.3.2. (document)

G. W. Inverarity. Correcting airborne temperature data for lags introduced by instruments with two-time-constant responses. *Journal of Atmospheric and Oceanic Technology*, 17 (2):176–184, 2000. doi: 10.1175/1520-0426(2000)017<0176:CATDFL>2.0.CO;2. URL https://doi.org/10.1175/1520-0426(2000)017<0176:CATDFL>2.0.CO;2. 1.1, 2.2

R. Paul Lawson and Alfred R. Rodi. A new airborne thermometer for atmospheric and cloud physics research. part i: Design and preliminary flight tests. *Journal of Atmospheric and Oceanic Technology*, 9(5):556–574, 1992. doi: 10.1175/1520-0426(1992)009<0556:ANATFA>2.0.CO;2. URL https://doi.org/10.1175/1520-0426(1992)009<0556:ANATFA>2.0.CO;2. 1.1, 1.1

D. H. Lenschow. The measurement of air velocity and temperature using the NCAR Buffalo Aircraft Measuring System. Technical report, 1972. URL http://nldr.library.ucar.edu/repository/collections/TECH-NOTE-000-000-000-064. 2.1

John McCarthy. A method for correcting airborne temperature data for sensor response time. *Journal of Applied Meteorology*, 12(1):211–214, 1973. 1.1, 2.1, 2.2

National Research Council. *The Atmospheric Sciences: Entering the Twenty-First Century*. The National Academies Press, Washington, DC, 1998. ISBN 978-0-309-06415-6. doi: 10.17226/6021. URL https://www.nap.edu/catalog/6021/the-atmospheric-sciences-entering-the-twenty-first-century. 1.1

G. A. Payne, C. A. Friehe, and D. K. Edwards. Time and frequency response of a resistance-wire aircraft atmospheric temperature sensor. *Journal of Atmospheric and Oceanic Technology*, 11(2):463–475, 1994. doi: 10.1175/1520-0426(1994)011<0463:TAFROA>2.0.CO;2. URL https://doi.org/10.1175/1520-0426(1994)011<0463:TAFROA>2.0.CO;2. 1.1, 2.1

David Pierce. *ncdf4: Interface to Unidata netCDF (Version 4 or Earlier) Format Data Files*, 2015. URL https://CRAN.R-project.org/package=ncdf4. R package version 1.15. (document)

R Core Team. *R: A language and environment for statistical computing*. R Foundation for Statistical Computing, Vienna, Austria, 2019. URL http://www.R-project.org. (document), 7, A

RStudio. *RStudio: Integrated development environment for R (Version 0.98.879)*, 2009. URL http://www.rstudio.org. (document), A

T. M. Stickney, M. W. Shedlov, and D. I. Thompson. Goodrich total temperature sensors. Goodrich Technical Report 5755 Revision C, Rosemount Aerospace Inc., 1994. URL http://www.faam.ac.uk/index.php/component/docman/doc_download/47-rosemount-report-5755(lastaccess:8Aug2014). 3.1.3

Bruce Swihart and Jim Lindsey. *rmutil: Utilities for Nonlinear Regression and Repeated Measurements Models*, 2019. URL https://CRAN.R-project.org/package=rmutil. R package version 1.1.3. (document)

UCAR/NCAR - Earth Observing Laboratory. NCAR/NSF C-130 navigation, state parameter, and microphysics HRT (25 sps) data. version 1.0 [data set, VOCALS], 2011. URL https://doi.org/10.5065/d69k48jk,Accessed09Jan2020. (document), A

UCAR/NCAR - Earth Observing Laboratory. High rate (hrt - 25 sps) navigation, state parameter, and microphysics flight-level data. version 2.0. [data set, CSET], 2017. URL https://doi.org/10.5065/D63R0R3W,Accessed12Mar2020. A

UCAR/NCAR - Earth Observing Laboratory. High rate (HRT - 25 sps) navigation, state parameter, and microphysics flight-level data. version 0.1 [preliminary] [data set, WE-CAN], 2018. URL https://data.eol.ucar.edu/dataset/548.004.Accessed09Jan2020. (document)

UCAR/NCAR - Earth Observing Laboratory. High rate (HRT) navigation, state parameter, and microphysics flight level data. version 1.0 [data set, SOCRATES], 2019. URL https://doi.org/10.26023/K5VQ-K6KY-W610,Accessed09Jan2020. (document), A

H. Wickham. *ggplot2: elegant graphics for data analysis*. Springer New York, 2009. ISBN 978-0-387-98140-6. URL http://had.co.nz/ggplot2/book. (document)

Y. Xie. *Dynamic Documents with R and knitr*. Chapman and Hall/CRC, Boca Raton, Florida, 2013. URL http://yihui.name/knitr/. ISBN 978-1482203530. (document), A

Y. Xie. *knitr: A general-purpose package for dynamic report generation in R*, 2014. URL http://yihui.name/knitr/. R package version 1.6. (document), A